


Three Cu (II)-hydrazone complexes: synthesis, physicochemical characteristics, stability, thermal analysis, and investigation of metal and iodine absorption

Ahmed A. Alzharani¹ 

Received: 14 March 2023 / Accepted: 13 May 2023

Published online: 31 May 2023

© The Author(s) 2023 

Abstract

A three Schiff bases; Lhy, Lme, and Lph, as well as their CuLhy, CuLme, and CuLph complexes, were synthesized, and their physicochemical properties were investigated. Vibrational spectra proposed that the hydrazone ligands reacted as neutral tridentate chelator with NNO chelating centers to the Cu(II) ion via azomethine-N, Isatin-carbonyl, and pyridine-N forming the general formulae $[Cu(L)_2]Cl_2 \cdot nH_2O$, where L = neutral tridentate Isatin-hydrazone ligand (L = Lhy, (CuLhy); L = Lme, (CuLme); L = Lph, (CuLph)). TG/DTA analyses have shown that there is at least one water molecule in each of the complexes. The spectrophotometric method was used to calculate the stoichiometry and thermodynamic characteristics of the metal complexes. By using density functional theory (DFT) techniques, the 3D structure of the produced complexes was verified. Based on an investigation of the electronic structural configurations of the complexes, calculations verified the predicted structure and clarified the nature of the chemical reactivity. Cu(II) adsorption from aqueous solutions onto ligands was investigated in a number of different settings. The influence of the initial metal concentration (10–100 ppm), the weight of the hydrazone ligands (0.1–1.0 gm), and the contact period (1–2 h) were all investigated as potential moderators of the uptake behavior. In just three hours, equilibrium had been reached thanks to the speedy adsorption process. An initial pH of $\approx 6-8$ with a metal ion concentration of 80 ppm was found to be optimal. Iodine (I_2) uptake behavior of hydrazone ligands was also studied using spectroscopy. In the first 8 h, hydrazone ligands exhibited high adsorption efficiency (E, %), which gradually declined until equilibrium was achieved after 25 h.

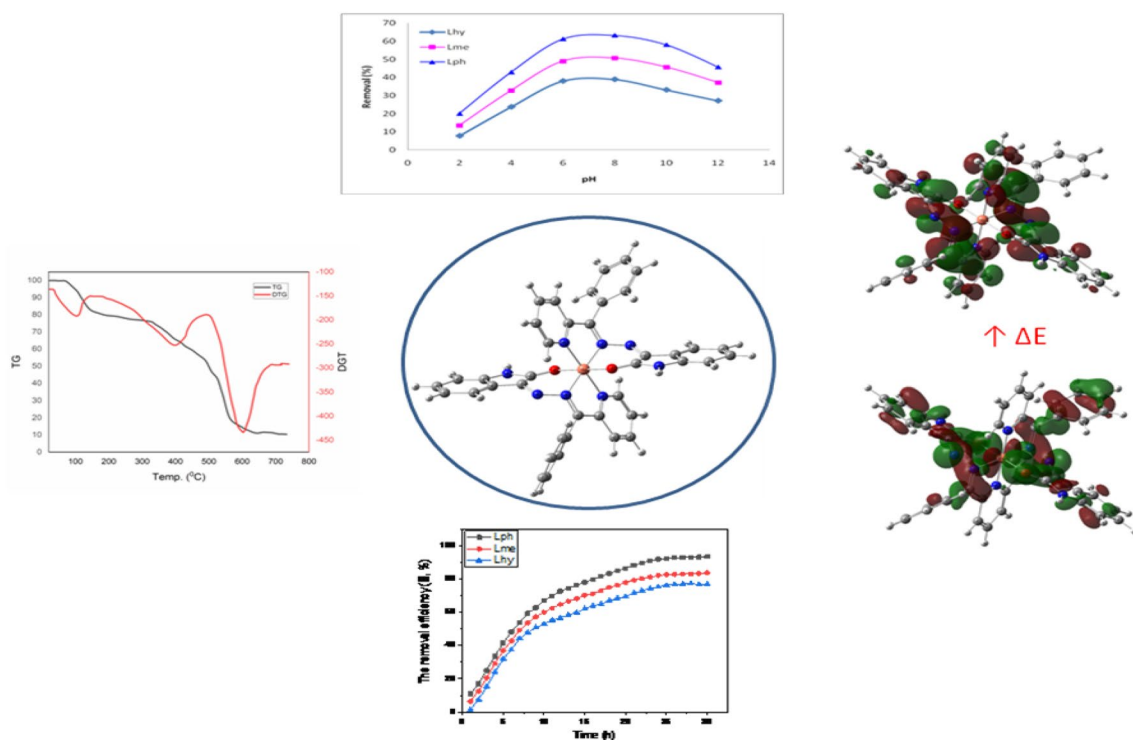
Supplementary Information The online version contains supplementary material available at <https://doi.org/10.1007/s43994-023-00054-5>.

✉ Ahmed A. Alzharani, aas.alzharani@bu.edu.sa | ¹Department of Chemistry, Faculty of Science, Al-baha University, Al Bahah 65799, Saudi Arabia.



J.Umm Al-Qura Univ. Appl. Sci. (2023) 9:455–470 | <https://doi.org/10.1007/s43994-023-00054-5>

Graphical abstract



Keywords Hydrazone ligands · Cu (II) complexes · Formation and stability constant · Metal uptake · Thermal analysis

1 Introduction

Hydrazones/Schiff-bases and their metal complexes are important in various fields [1] such as cytotoxicity [2, 3], analytical [4, 5], catalytic [6], optoelectronic [7], photore-sponse [8], biomedical and wastewater remediation [9] studies. Moreover, they had been used as antioxidant [10], chemotherapeutic [11], antimicrobial [12], antiproliferative [13], and antitumor agents [14]. In addition to its use in inorganic chemistry, materials science, Langmuir films, electrochemical sensors, and drastically increasing bioactivity [15], Hydrazones/ Schiff-bases and their associated metal complexes have a wide range of potential applications in other fields. Several branches of chemistry have been motivated to develop metallic complexes due to the benefits they provide. These ligands were tested in a wide range of stimulatory, anticancer, and antibacterial tests [16, 17] due to their potent biological effect.

Heavy metal toxins found in wastewater from industrial processes are a significant contributor to environmental degradation [18]. Electroplating, pigment manufacture, metallurgical operations, mining, and the leather trade are just few of the many businesses that contribute

to the release of metals into the environment, and each of these industries releases metals at a different concentration [19]. Copper, cadmium, zinc, manganese, chromium, lead, and iron are some of the metal ions that are often found in natural and industrial effluents respectively [20]. These metal cations can be introduced into wastewaters by a wide variety of sources, some of which are listed below: catalysts, painting, electrical equipment and insecticides; antibacterial, coating, photography, and fungicides; metal electroplating; pigments; pyrotechnics; fertilizer; smelting; mining; electrical wiring; alloy industries; plumbing; heating; and water purification; and many others.

Heavy metal ion pollution is a growing concern because of the metals' severe toxicity and inertness. Metal ions may be removed from effluents by a variety of common treatment processes, including filtration [21], membrane technology [22, 23], chemical precipitation [24, 25], ion exchange [26], chemical coagulation [27], reverse osmosis [28, 29], and solvent extraction [30, 31]. These methods are expensive to run and only marginally effective in removing hazardous metal ions at trace amounts [32].

Potential methods include the use of chelating resins. When it comes to sorption processes, chelating resins are superior than ion exchange resins and activated carbon because of their superior selectivity and rapid regeneration after being exposed to metal ions [33]. Several studies [34] were described, discussing a broad range of chelating resins. There are many different interesting and important properties of Schiff bases that had been investigated. These include their reversible oxygen binding [35, 36], olefins hydrogenation [37], photochromic properties [38], and adsorption ability towards some toxic metals [39].

Those with preexisting thyroid conditions, the elderly, foetuses, and infants are more vulnerable to the effects of iodine poisoning, which may manifest as either subtle or obvious thyroid dysfunction in these populations. Effects of ingesting too much iodine may differ from one person to the next, depending on their baseline thyroid health. Iodine overdose may result in many thyroid disorders, such as thyroiditis, hypothyroidism, hyperthyroidism, and papillary thyroid cancer. Clinical signs of iodine toxicity after ingestion vary widely in severity. Stomach pain, nausea, vomiting, and diarrhoea are all minor side effects. These symptoms, if untreated, may progress to a state of delirium, stupor, or even shock. Becoming dangerous is incredibly rare.

The current study included the preparation and use of three Schiff bases for the adsorption of Cu(II) ion in aqueous environments. Contact time, pH, starting [Cu(II)] concentrations and adsorbent dose, were studied as they pertain to the removal process. The capability of the synthetic ligands to remove iodine was also tested.

2 Methodology

2.1 Materials and methodology

The materials, methods, and instruments which used in the preparation and characterization of the prepared compounds were listed in the supplementary information file.

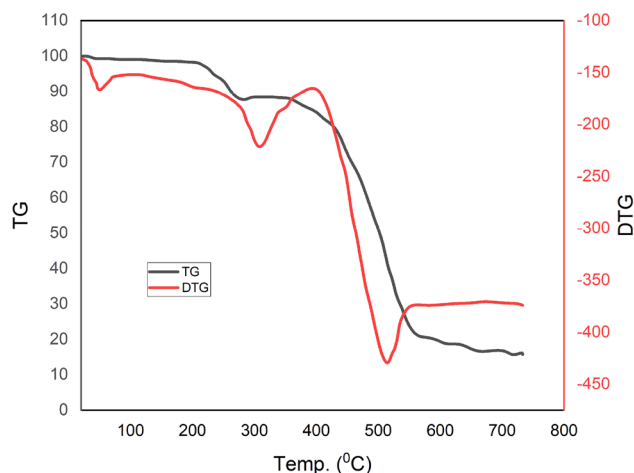
2.2 Preparation

2.2.1 Preparation of the Lhy, Lme and Lph ligands

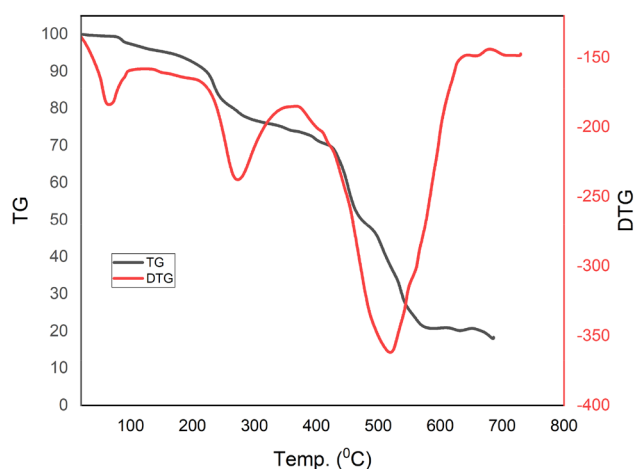
The two stages required preparing Lhy, Lme and Lme are as follows: hydrazone ligands were synthesized by first preparing monohydrazone, and then reacting it with (Pyridine-2-carboxaldehyde, 2-acetyl pyridine, 2-benzoyl pyridine,), as described in Fig. 1.

Hydrazine hydrate solution (0.1 g, 20 mmol) in ethanol (25 mL) was combined with a solution of isatin (2.94 g, 20 mmol) dissolved in ethanol (25 mL). After that, the

CuLhy Complex



CuLme Complex



CuLph Complex

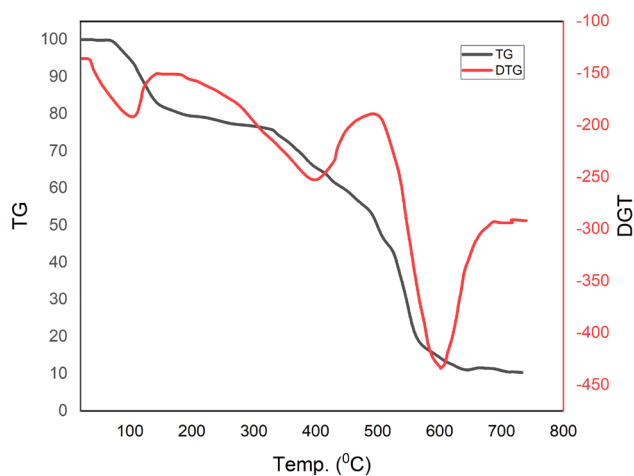
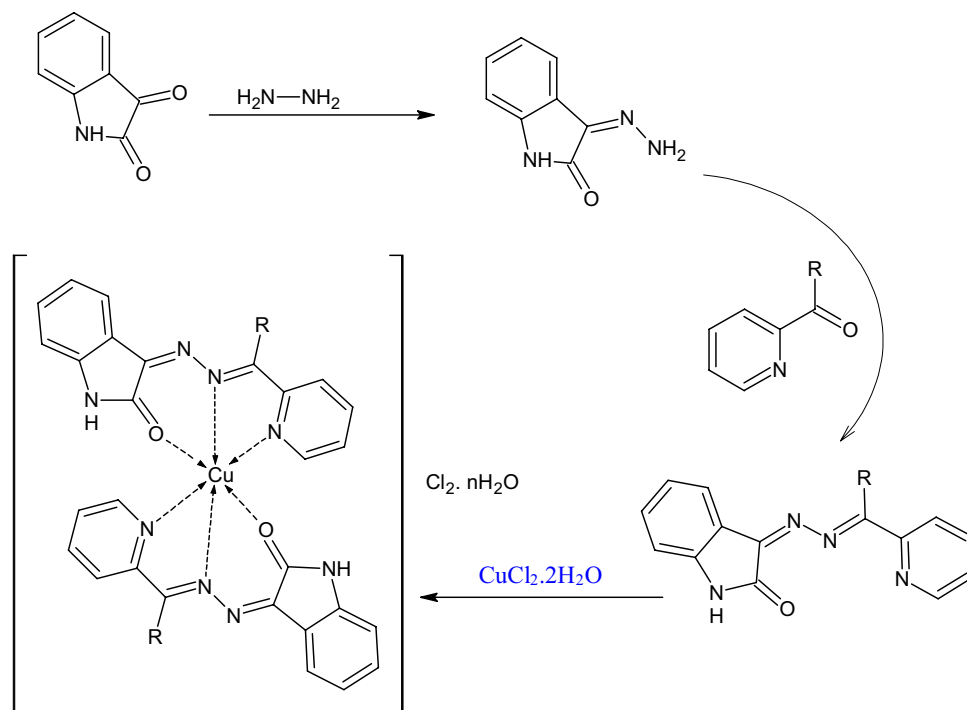


Fig. 1 Thermal decomposition of the CuLhy, CuLme, and CuLph complexes

Scheme 1 Schematic diagram of the Lhy, Lme, and Lph ligands preparation and their Cu(II)- complexes



resultant brew was given four hours of reflux treatment in a water bath. The resulting yellow chemical was filtered, washed with cold ethanol, dried, and re-crystallized from ethanol after cooling.

Hot ethanolic monohydrazone solution (2.0 mmol) was added drop wise with 2-pyridyl (2-acetyl pyridine, 2-benzoyl pyridine, Pyridine-2-Carboxaldehyde), and the resultant mixture was refluxed for 10 h with steady magnetic stirring. After forming, a ligand is cooled, filtered, washed in cold ethanol, dried, and then re-crystallized [40].

2.2.2 Preparation of Cu(II) complexes

Following this general procedure, solid Cu(II) chelates of hydrazone ligands were synthesized by adding a the metal salt solution [$\text{CuCl}_2 \cdot 6\text{H}_2\text{O}$, 2.0 mmol] in minimal water amount drop by drop to an ethanolic ligand solution [Lhy or Lme or Lph, 2.0 mmol] and then refluxing the mixture at 80 °C for 12 h with fixed stirring, Scheme 1. After evaporating the product overnight, it was filtered and washed. The purity of the synthesized compounds was monitored by TLC using silica gel-G. All the metal complexes are stable in air, non-hygroscopic and melt above 300 °C.

2.3 Stoichiometry and complexes formation constant

These compounds' stoichiometries were calculated using the spectrophotometric molar ratio [41–43] and continuous variation techniques [44, 45]. The controversial

variation procedure applied to analyze the formation constant was repeated across a broad range of temperatures (20 to 40 °C) to find out the thermodynamic characteristics and the formation constant of the prepared chelates.

2.4 DFT calculations

DFT computations were carried out to verify the hypothesised geometrical structures of the Cu(II) hydrazone complexes. We used the B3LYP and the LANL2DZ basis set to optimize the geometry [46, 47]. The computations were done using the Gaussian 09 software package. The structures of the CuLhy, CuLme, and CuLph complexes of three hydrazone ligands, Lhy, Lme, and Lph, were calculated [48–50].

2.5 Metal ion uptake study

Shaking 0.6 g of the hydrazone ligands with 10 mL (80 ppm) of Cu(II) solution of varied pH values (2–12) for 1 h at 25 °C was used for the uptake tests in the influence of pH research. We used buffers to get the solution pH exactly right.

A series of closed conical flasks were filled with 10 mL (80 ppm) of Cu(II) at pH 8, and 0.6 g of the produced hydrazone ligands was added. Several contact times (0.5 h, 1 h,.... 3 h) were tested in the batch sorption investigations. A mechanical shaker was used to agitate the flask's contents at room temperature. After shaking, each sample

was filtered separately before atomic absorption analysis of metal ion concentration in solution (AA).

Placed of hydrazone ligands (0.6 g) in a series of flasks holding 10 mL of Cu(II) at pH 8 and specified concentrations (10–100 mg/L), to test the influence of starting concentration of the Cu(II) ion on the absorption of Cu(II) ions by the ligands. During 60 min, the flasks were set on the shaker at at 25 °C to allow the contents to acclimatise. The samples were filtered after adsorption, and the metal ion concentration was measured by atomic absorption spectroscopy (AA).

Measurements of Cu(II) ion absorption using the batch technique were carried out by adding various adsorbent weights (0.2 g to 1.0 g, 0.5 g) to 10 mL (80 ppm, pH 8) of Cu(II) ions solutions in a series of stopper conical flasks. During 60 min at room temperature, the flask contents were shaken on a shaker.

The proportion of metal ion removal in all batch sorption investigations was calculated using the following formula; Removal (%) = $((C_0 - C_e)/C_0) \times 100$. Metal ion concentration at equilibrium (C_e), the starting concentration (C_0).

2.6 Adsorption of iodine

The adsorption of iodine onto hydrazone ligands was studied using batch experiments: (a) 100 mg of ligands were placed in a sealed vessel with 100 mg/L of iodine/hexane solution (20 mL) and left for a set amount of time; (b) the absorbance of the supernatant in the anterior vessel was measured at 525 nm using UV–vis at different times.

The following formulae were used to determine the adsorption effectiveness (E , %) and the iodine adsorbed quantity (q_e , mg/g) [51]: $q_e = (C_0 - C_e)V/m$, $E(\%) = ((C_0 - C_e)/C_0) \times 100\%$; Where C_0 and C_e are the starting and final

iodine concentrations in milligrammes per litre, m is the hydrazone ligand quality in grammes, and V is the concentration of the solution (L).

3 Results and discussion

First, isatin interacted with hydrazine by water molecule elimination to generate isatin-mono hydrazone, which then reacted with 2-substituted pyridine through water molecule elimination to form the hydrazone ligands (Lhy, Lme, and Lph), Scheme 1. Second, Cu(II)-hydrazone complexes (CuLhy, CuLme, and CuLph) were formed when the hydrazone ligands (Lhy, Lme, and Lph) coordinated with the Cu(II), Scheme 1.

3.1 Characterization of the hydrazone ligands

The characterization of the prepared hydrazone ligands were listed in the supplementary information file.

3.2 Characterization of the CuLhy, CuLme, and CuLph complexes

3.2.1 Conductivity and elemental analysis

The tridentate hydrazones (Scheme 1) are produced via the condensation of isatin monohydrazone with 2-pyridyl. The solid, non-hygroscopic character of these CuLhy, CuLme, and CuLph complexes were shown by their presence in Scheme 1. The molar conductivity was measured for 1 mmol of the title complexes in Ethanol solution. The values of molar conductivity indicated 1:2 electrolytic character for all the three complexes. Analytical data

Table 1 Analytical physical data of the Lhy, Lme, and Lph ligands and CuLhy, CuLme, and CuLph complexes

	Color	Yield (%)	m.p (°C) (%)	Elemental analysis found (calculated)				μ_v ($\Omega^{-1} \text{ cm}^2 \text{ mol}^{-1}$) Ethanol
				C %	H %	N %	M %	
Lhy $\text{C}_{14}\text{H}_{10}\text{ON}_4$ (250 g/mol)	Orange	240 °C	85	67.41 (67.21)	4.42 (4.29)	22.21 (22.34)	–	–
CuLhy [Cu(Lhy) $_2$]Cl $_2$ 0.2H $_2$ O ($\text{C}_{28}\text{H}_{24}\text{Cl}_2\text{CuN}_8\text{O}_4$, 670.5 g/mol)	Green	> 300	72	50.58 (50.12)	3.50 (3.61)	16.79 (16.70)	9.36 (9.47)	85
Lme $\text{C}_{15}\text{H}_{12}\text{ON}_4$ (264 g/mol)	Orange	254 °C	86	68.11 (68.48)	4.44 (4.28)	21.12 (20.96)	–	–
CuLme [Cu(Lme) $_2$]Cl $_2$ 0.2H $_2$ O ($\text{C}_{30}\text{H}_{28}\text{Cl}_2\text{CuN}_8\text{O}_4$, 698.5 g/mol)	Green	> 300	75	51.10 (51.54)	3.99 (4.04)	16.15 (16.03)	8.95 (9.09)	81
Lph $\text{C}_{20}\text{H}_{14}\text{ON}_4$ (326 g/mol)	Orange	266 °C	86	73.66 (73.53)	4.39 (4.29)	17.20 (17.03)	–	–
CuLph [Cu(Lph) $_2$]Cl $_2$ 0.2H $_2$ O ($\text{C}_{40}\text{H}_{32}\text{Cl}_2\text{CuN}_8\text{O}_4$, 822.5 g/mol)	Green	> 300	77	58.55 (58.36)	3.65 (3.92)	13.60 (13.61)	7.78 (7.72)	88

(Table 1) and spectrum examinations showed the ligands and CuLhy, CuLme, and CuLph complexes to be of high purity, as was expected.

3.2.2 IR spectra and mode of bonding

Without access to more advanced methods like single X-ray crystallography, infrared spectra have emerged as the most useful tool for deciphering ligand–metal ion interaction. The supplementary information table (S1) below lists the visible and IR spectral lines of the ligands and related Cu(II) complexes. These bands may be broken down into two categories: those caused by the ligands, and that caused by the bonds between the Cu(II) and the coordinating centers. Bands at 3180–3200 cm^{-1} and 1722 cm^{-1} in the IR spectrum of the hydrazones may be attributed to the (–NH) and lactonyl carbon $\nu(\text{C}=\text{O})$, respectively [52]. Moreover, the IR spectra of the ligands attribute the band at 1461 cm^{-1} to $\text{C}=\text{N}$, and the typical strong band at 1620 cm^{-1} to $\text{HC}=\text{N}$. All of the CuLhy, CuLme, and CuLph complexes displayed the band of ($\text{HC}=\text{N}$) in the area 1591 cm^{-1} , displaying lower wave numbers shift of the band suggesting that, the ($\text{CH}=\text{N}$) nitrogen is binding to the Cu(II) ion [53, 54], in contrast to the spectra of the ligands. The carbonyl oxygen is binding to the Cu(II) ion, as seen by the lower wave number shift in the band of ($\text{C}=\text{O}$) in the area 1674–1683 cm^{-1} in CuLhy, CuLme, and CuLph complexes [54, 55]. There is no evidence of coordination activity from the –NH group, since its presence does not shift the location of a band in any of the metal complexes. We attribute the appearance of new bands in the complexes' spectra at 500–510 cm^{-1} and 630–650 cm^{-1} to the stretching frequencies of ($\text{M}-\text{N}$) and ($\text{M}-\text{O}$) bonds, respectively [56]. That ligands complex with Cu(II) ion in tridentate mode is supported by IR spectrum data is so conclusive.

3.2.3 Electronic spectra

Coordination chemists may use electronic spectra to learn crucial details about the complexes' structures. Due to conjugation, the UV absorption bands of the ligands, which are organic molecules, might expand into the higher wavelength range. The addition of metal ions causes a shift in the system's electronic characteristics. Seeing the appearance of new features or bands in the visible region as a result of d-d absorption and charge transfer spectra from metal to ligand (ML) or ligand to metal (LM) allows one to deduce structural and geometrical information about the complexes. In MeOH ($1 \times 10^{-3} \text{ mol/dm}^3$), the UV–vis. spectra of Lhy, Lme, and Lph ligands and their Cu(II)-complexes were obtained from 200 to 800 nm. You can find a supplementary information table (S1) with the

absorption maxima in it. The $\pi-\pi^*$, $n-\pi^*$ transitions [53] in the UV–Vis spectra of the Lhy, Lme, and Lph ligands gave two prominent, bright bands at (237 and 324), (274 and 325) and (271 and 327), respectively. Complexation further modifies these bands. In three copper complexes one band at 18,181.82–17,543.86 cm^{-1} is due to d-d transitions and the spectrum also displayed another band in the range 24,390.24–23,809.52 cm^{-1} . This band corresponded to the transition ${}^2\text{B}_{1g} \rightarrow {}^2\text{A}_{1g}$.

3.2.4 Complexes stoichiometry and formation constants

With the use of spectrophotometric molar ratio [41, 43, 57] and continuous variation [44, 58] techniques, the stoichiometry of the different complexes produced in solution by the interaction of Cu(II) with the investigated hydrazone ligands was evaluated (supplementary information Figure (S1)). Continuous variation method curves showed maximum absorbance at mole fraction of the ligand = 0.65–0.7, suggesting complex formation at a Cu(II) to ligand ratio of 1:2 ((supplementary information Figure (S1)). The ratio of metal ions to ligands in the produced complexes (see supplementary information Figure (S1)) is also supported by the molar ratio approach.

Using the continuous variation approach on spectrophotometric observations, the formation constants (K_f) of the investigated Cu(II) hydrzone complexes produced in solution were calculated, $K_f = (A/A_m) / [4C_2(1 - (A/A_m))]^3$ [59]:

Where A_m is the absorbance at maximal complex formation, A is the actual absorbance of the complex, and C is the starting Cu(II) concentration. Supplementary information Table S2 shows that the obtained K_f values, which demonstrate the produced complexes' exceptional stability, are impressive. For the investigated complexes, K_f values rise as (CuLph > CuLme > CuLhy).

The Gibbs–Helmholtz equation, $\text{Log}K_f = \frac{\Delta S^*}{2.303R} - \frac{\Delta H^*}{2.303R T}$ was used to calculate the free energy (ΔG^*), enthalpy (ΔH^*), and entropy (ΔS^*) changes that occur as a result of a complexation process [60].

One may evaluate (ΔH^*) and (ΔS^*) using the slope and intercept of a straight line obtained by graphing the values of ($\text{Log}K_f$) against ($1/T$), respectively. Calculated values for ΔG^* , ΔH^* , and ΔS^* are listed in Supplementary information Table S2.

The enthalpy (ΔH^*) change is negative, thus, the reaction happened is exothermic and creation of complex is favourable [61]. Negative amount of enthalpy change also shows that the Cu(II)-ligand bonds are quite strong [62]. As ΔS^* is greater than zero, the reaction is likely to continue on its own [63]. The liberation of water molecules bound to metal chelates is the cause of the positive entropy changes that occur alongside a particular process. The production

Table 2 Thermal decomposition of the Cu(II) complexes

	Step	T.G (°C)	DTG (°C)	Mass loss: Obs. (Calc.) (%)	Assignment	Residue
CuLhy	I	50–110	88	5.83 (5.37)	2H ₂ O (hydrated)	CuO
[Cu(Lhy) ₂]Cl ₂ 2H ₂ O	II	110–395	310	12.18 (12.67)	CH ₂ Cl ₂	
(C ₂₈ H ₂₄ Cl ₂ CuN ₈ O ₄ , 670.5 g/mol)	III	395–600	505	72.83 (72.48)	C ₂₇ H ₁₈ N ₈ O ₂	
CuLme	I	50–115	95	5.78 (5.15)	2H ₂ O (hydrated)	CuO
[Cu(Lme) ₂]Cl ₂ 2H ₂ O	II	115–405	320	12.68 (12.17)	CH ₂ Cl ₂	
(C ₃₀ H ₂₈ Cl ₂ CuN ₈ O ₄ , 698.5 g/mol)	III	405–600	520	71.93 (71.29)	C ₂₉ H ₂₂ N ₈ O ₂	
CuLph	I	50–150	105.55	4.85 (4.38)	2H ₂ O (hydrated)	CuO
[Cu(Lph) ₂]Cl ₂ 2H ₂ O	II	150–460	350.43	10.02 (10.33)	CH ₂ Cl ₂	
(C ₄₀ H ₃₂ Cl ₂ CuN ₈ O ₄ , 822.5 g/mol)	III	460–600	500.55	76.04(75.62)	C ₂₉ H ₂₂ N ₈ O ₂	

of metal chelates involves the displacement of water molecules from the metal ion's main hydration sphere [62].

Williams noted that the displacement of solvent water molecules during the combination of positively charged metal ions and ligands was often accompanied by a high entropy value [64]. The entropy is low because the water molecules that are coupled to the metal ions are extremely twisted and orientated.

3.2.5 Thermo-gravimetric study of the prepared isatin-hydrazone complexes

Potential biological actions of the hydrazone ligands (Lhy, Lme, and Lph) underline the significance of this research into their Cu(II) complexes. This is why thermal analysis and other physicochemical techniques are often used to learn more about them. Determining the total amount of water molecules and how well they are hydrated and coordinated allows for a perfect deduction of the complicated structure.

Table 2 provides information on the complexes' temperatures. hydrazone CuLhy, CuLme, and CuLph complexes are thermally stable between 25 and 50 °C, and thereafter deteriorate in three stages. Figure 1 suggests that the thermal degradation occurs in three steps, the first of which occurs between 50–110 °C (CuLhy), 50–115 °C (CuLme) and 50–150 °C (CuLph), corresponding to loss of two hydrated water molecules. The second stage, at 110–395 °C (CuLhy), 115–405 °C (CuLme) and 150–460 °C (CuLph), may be attributed to the loss of CH₂Cl₂ molecule. The third, at 395–600 °C (CuLhy), 405–600 °C (CuLme) and 460–600 °C (CuLph), corresponds to loss of the remaining organic moiety, leaving CuO as metallic residue.

From Thermal analysis (TG) data, it is suggested that the final residue content of the Cu(II) complexes is CuO, according to overall mass loss. Based on the thermal analysis, CuO can be prepared by calcinations the Cu(II) complexes as precursors at ≈ 500 °C. Therefore, the choice of

suitable calcinations temperature is highly dependent on the results of thermal analysis. The final residue content is CuO is characterized by FT-IR spectroscopy. The samples show absorption maxima at 503, 499, and 495 cm⁻¹ for CuO prepared from CuLhy, CuLme, and CuLph complexes, respectively, which are due to Cu–O stretching mode [65, 66].

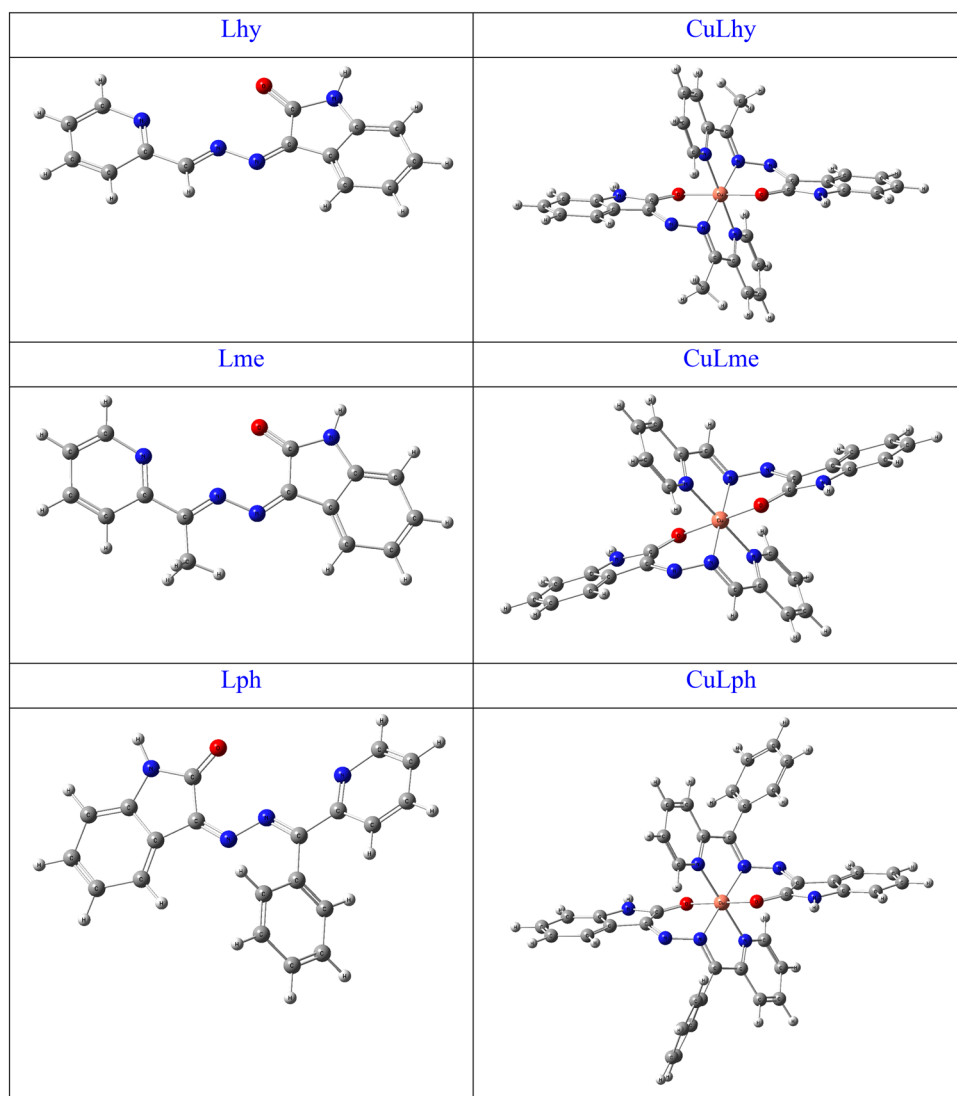
3.2.6 Effective magnetic moment

The effective magnetic moment values of the [Cu(Lhy)₂]Cl₂ 2H₂O (CuLhy), [Cu(Lme)₂]Cl₂ 2H₂O (CuLme), and [Cu(Lph)₂]Cl₂ 2H₂O (CuLph) complexes were found to be 1.78, 1.75, and 1.77 B.M., respectively. These values are consistent with one unpaired electron (d⁹ (t_{2g}⁶ e_g³)) around the Cu(II) centre [67, 68], which confirmed the octahedral geometry with sp³d² hybridization [69].

3.3 Theoretical modeling of Cu(II) hydrazone complexes

The dihedral angle between the carbonyl oxygen, azomethine nitrogen, and pyridine nitrogen, as determined by the optimized structure of the ligands, is 160.0 degrees, indicating that these atoms all have a similar orientation. Because of its unique orientation, the ligand is able to create an aromatic-like structure with the metal ion. The optimum structures of CuLhy, CuLme, and CuLph complexes with Lhy, Lme, and Lph ligands are shown in Fig. 2. Copper(II) was found to coordinate with the ligands in an octahedral fashion, as determined by the optimization process. In particular, the carbonyl group, azomethine group, and pyridine group linked the metal atoms together. In order to achieve octahedral coordination, it was determined that the average bond length for the (Cu-ligand link is 1.83. Two aromatic five- and six-ring structures are created between the Cu and the ligand molecule, and this is the primary reason for

Fig. 2 Optimized structures of the Lhy, Lme and Lph ligand models and their corresponding CuLhy, CuLme, and CuLph complexes calculated using DFT method



the produced complexes' exceptional stability. The coordination (N–Cu–N) angle computed for the previous five-membered ring was 88.5 degrees. The computed coordination (O–Cu–N) angle for the other six-membered ring was 100.0 degrees as well.

Materials scientists, physicists, and chemists may learn a great deal by studying LUMOs and HOMOs and the features of these molecular states [70]. Figure 3 depicts the HOMO and LUMO surfaces. The stability of compounds is determined by the negative values of their HOMO and LUMO energies. Global chemical reactivity descriptors (HOMO, LUMO, energy gap, chemical hardness, electronic chemical potential, and electrophilicity) were computed to quantify the relative stability and chemical reactivity of the predicted complexes [71–73]. Here is a definition of what these terms represent in a physical sense: The chemical hardness (η) of a molecule is defined as its ability to withstand a change in the distribution of its electrons or a

change in its net charge. The degree to which a molecule is negatively charged is quantified by its electronic chemical potential (μ). This species' willingness or ability to receive electrons is quantified by an electrophilicity index (ω). The estimated chemical descriptors for all models are summarized in Table 3.

The stability and reactivity of a chemical system are related to its hardness (η). Chemical hardness is defined as the difference in energy between the HOMO and LUMO orbitals at the molecular border. Higher energy gaps indicate that molecules are more robust and less prone to chemical reactions. The estimated complexes with the biggest and smallest values for are CuLph and CuLhy, respectively. The stability constant determined experimentally is consistent with these findings. Similar hues and a small range in λ_{\max} for complexes account for the little variation in results.

Fig. 3 HOMO–LUMO structures of the Lhy, Lme and Lph ligands CuLhy, CuLme, and CuLph complexes calculated using DFT method

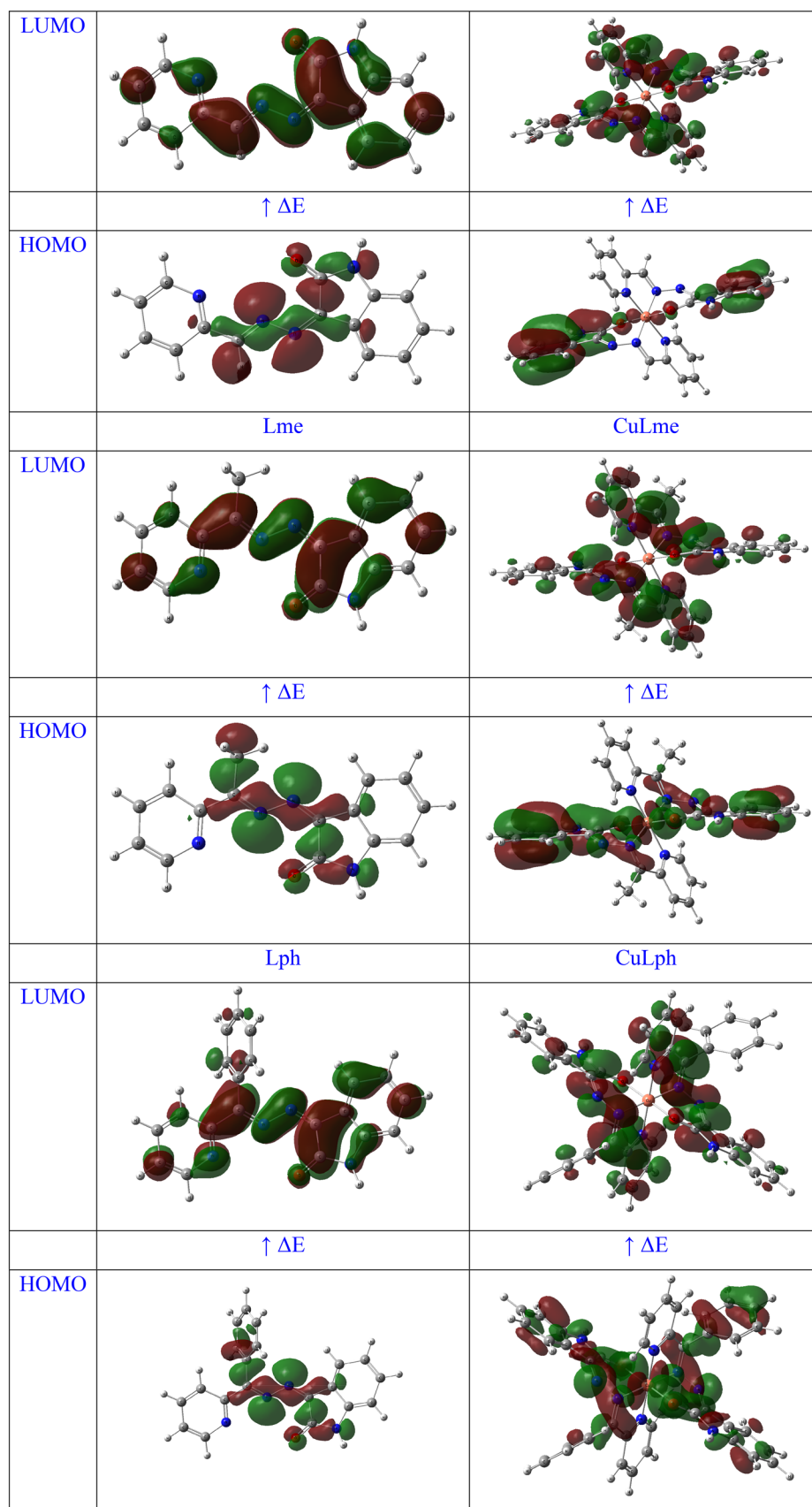


Table 3 HOMO, LUMO, ΔE , η , μ and ω of the Lhy, Lme, and Lph and their Cu(II) complexes

Model	HOMO	LUMO	ΔE	η	μ	ω
Lhy	– 6.15	– 2.32	3.83	1.92	– 4.24	4.68
Lme	– 6.07	– 2.25	3.82	1.91	– 4.16	4.53
Lph	– 6.07	– 2.34	3.73	1.87	– 4.21	4.74
CuLhy	– 12.90	– 11.31	1.59	0.80	– 12.11	92.16
CuLme	– 12.82	– 10.42	2.40	1.20	– 11.62	56.26
CuLph	– 4.08	– 1.61	2.47	1.24	– 2.85	3.28

3.4 Metal uptake

In Fig. 4a we saw how the metal ion absorption onto the hydrazone ligands changed as a function of contact time. The figures of % removal were shown to grow significantly at the start of adsorption, but after 3 h, the rate of change slowed down. As a result, the metal ion was rapidly adsorbed. The metal ion adsorption amount hardly changed after around 3 h. This pattern of action suggests a sluggish journey towards balance.

Alternatively, the effect of hydrazone ligands' weight on Cu(II) ions sorption was studied. Solid hydrazone ligands of known weights were added to a known concentration of Cu(II) ion (100 ppm) to achieve a range of weight values (0.1–1.0 gm). Obtaining these findings was shown in Fig. 4b. Maximum metal ion removal % was observed at a hydrazone ligands weight of 0.6 gm. Also visible is the correlation between the weight of the hydrazone ligand and the quantity of metal ion adsorbed.

Adsorption behaviour of produced hydrazone ligands towards Cu(II) ion was studied, and the findings are shown in Fig. 4c. At low concentrations, Cu(II) is taken up by specific active centers; at higher concentrations, the binding centers become more rapidly saturated as the ligands amount increased, making the metal uptake mechanism particularly dependent on the initial Cu(II) concentration. The Cu(II) ions uptake rises linearly with increasing starting concentration up to a plateau. The solutions pH was changed to various values using appropriate buffers to investigate the impact of pH on Cu(II) ion removal efficiency, with the range being from 2.0 to 12.0 for Cu(II). Figure 4d shows that the ideal pH for efficient metal removal is related to the absorption of free ionic Cu (II). Copper (II) concentrations in the various solutions were accurately measured both before and after 60 min of vigorous shaking. The removal efficiency was computed and the findings obtained were depicted in Fig. 4d. According to the results, the proportion of Cu (II) that was removed varied with the test solution pH between 2 and 12, with the highest adsorption affinities occurring between pH 6 and 8. This behavior makes sense given that hydrogen ions may

compete with Cu(II) ions for active centers on the surface of Lhy, Lme, and Lph ligands when the medium is acidic. Electrostatic repulsion between the Cu(II) and the protonated groups may hinder the adsorption of the Cu(II) onto the resin at low pH, when most of the active functional groups in the hydrazone ligands were ionized and presented in the protonated positively charged state. Little amounts of Cu(II) have begun to accumulate as hydroxides, rendering metal ion retention practically steady between pH 6 and 8. This further helps the cations on the hydrazone ligands to become chelated. The optimal range for this chelation is between pH 6 and 8.

3.5 Removal of dissolved iodine by hydrazone ligands

Using solutions of cyclohexane at varying concentrations, we have examined the usefulness of hydrazone ligands. UV–Vis spectroscopy at 525 nm, pH = 7, was used to track the iodine elimination process.

While studying iodine absorption by hydrazone ligands, we found that during the first 8–10 h, the rate of uptake climbed rapidly, before gradually slowing to reach equilibrium. The saturation of iodine adsorption over hydrazone ligands was attained at 25 h, Fig. 5. This is because, initially, a large number of active sites were exposed on the surface of the ligands, leading to a sharp increase in the adsorption rate in the first 8–10 h. However, as time progressed, the active sites and the pores gradually became occupied and blocked, leading to a slowing of the adsorption rate.

As can be shown in Fig. 5, the order of Lph > Lme > Lhy describes the removal efficiency degree of the hydrazone ligands.

3.6 Adsorption isotherm

Langmuir and Freundlich models were used to fit the absorption isotherms and obtain insight into the absorption process for Cu(II) or I₂ (Fig. 6). In order to create the Langmuir isotherm, we plotted the adsorption capacity of the hydrazone ligands (mg/g) as (1/qe) against the

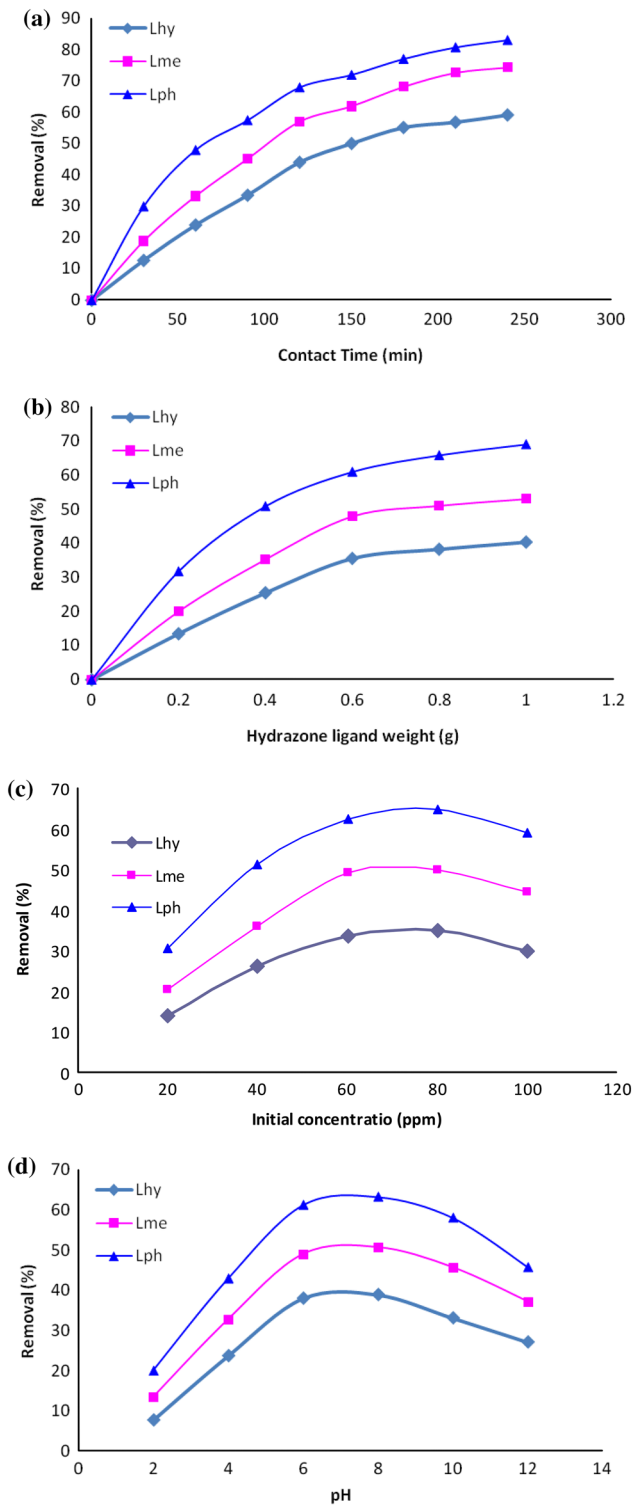


Fig. 4 **a** Effect of the contact time on the removal of Copper (II) ion using hydrazone ligands. **b** Effect of hydrazone ligands weight on metal ion removal, **c** effect of initial metal ion concentrations on metal ion removal using hydrazone ligands, **d** Effect of the pH on the removal of Copper (II) ion using hydrazone ligands

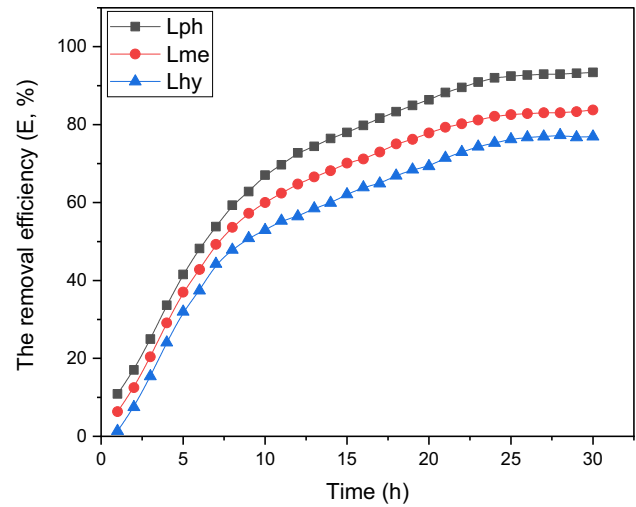


Fig. 5 The removal efficiency (E, %) of iodine using hydrazone ligands, at pH=7, amount of hydrazone ligands= 100 mg

equilibrium concentration of Cu(II) or I₂ (mg/L) as (1/Ce) to get a linear relationship between the two. Monolayer coverage over a uniform surface with the same number of adsorption sites and the same adsorption activation energy is a key tenet of the Langmuir model. To further investigate the iodine adsorption mechanisms, we plotted Ln(qe) vs Ln(Ce) to evaluate the Freundlich model (Fig. 6).

The findings reveal that the adsorption isotherms may be successfully suited by the Langmuir model, as shown by strong correlation coefficients (R²) of linearly fitted Langmuir isotherm models. The Freundlich model, in contrast to the Langmuir model, posits heterogeneous multilayer interaction and reversible adsorption.

Our findings are reported in Fig. 6, which shows that the linear fitted Langmuir isotherms have greater correlation coefficients than those obtained for fits to the Freundlich model. The adsorption isotherms for Cu(II) and iodine appear to be well described by both models, with somewhat good correlation coefficients.

3.7 Kinetic model

The findings of the kinetics analysis were obtained by fitting to the pseudo-first-order, $\ln [q_e - q_t] = \ln q_e - k_1 t$, and pseudo-second-order, $\frac{t}{q(t)} = \frac{t}{q_e} + \frac{1}{k_2 q_e^2}$, equations [74].

Where qt is the time-dependent adsorption capacity, qe is the equilibrium adsorption capacity, k1 is the pseudo-first order rate constant, k2 is the pseudo-second order rate constant, and t is the contact duration (Fig. 7).

Adsorption kinetics for Cu(II) and iodine are best described by a pseudo-first-order kinetic model for

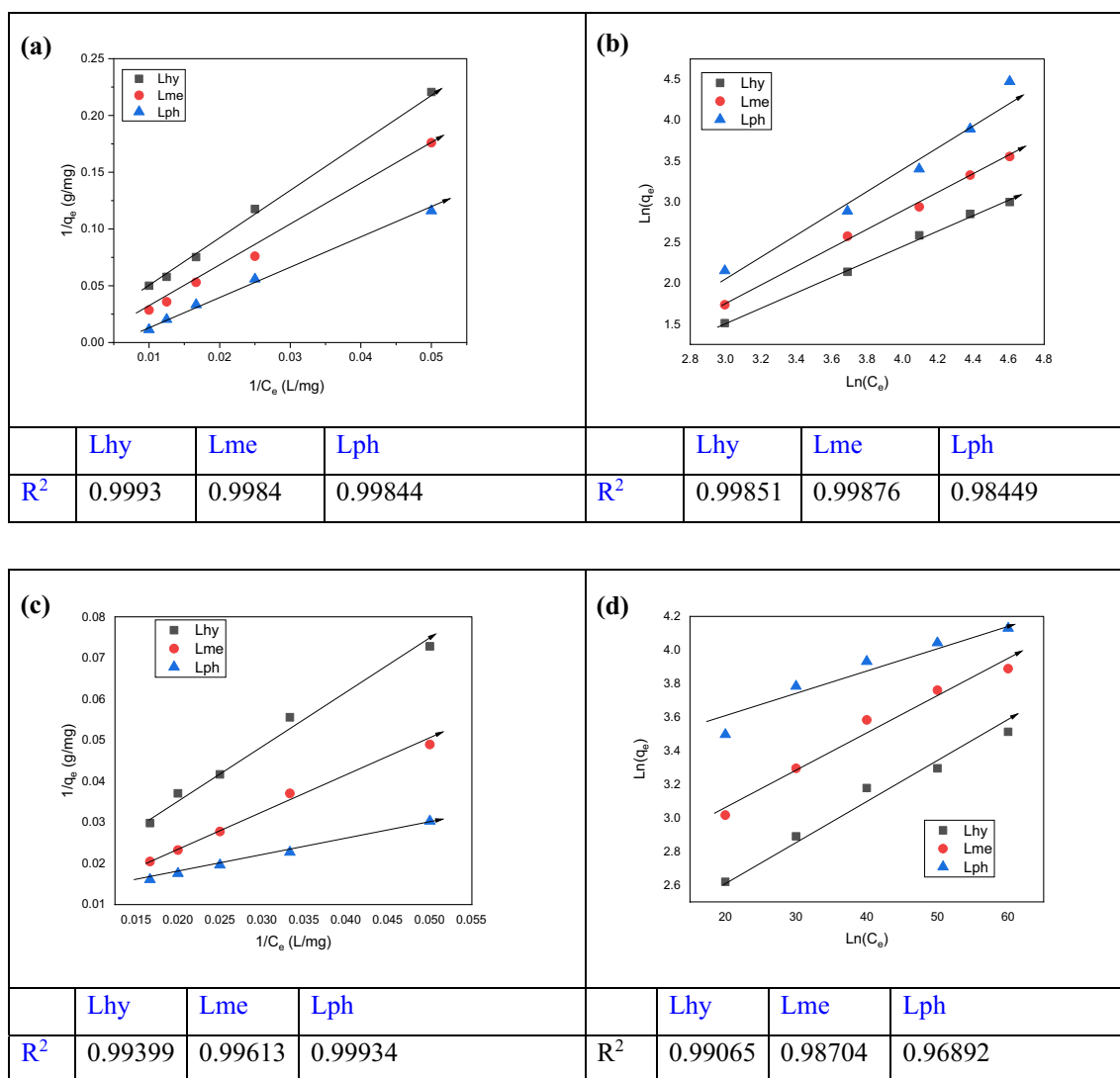


Fig. 6 Langmuir model for Cu(II) (a) and for I₂ (b); Freundlich model for Cu(II) (c) and for I₂ (d)

hydrazone ligands, as shown by the R^2 values derived (Fig. 7). These findings point to a chemisorption mechanism for the adsorption of Cu(II) and iodine [75, 76]. This is due to the intense bonding between the iodine molecules and the hydrazone-ligand surfaces. To increase their ability to capture Cu(II) and iodine, hydrazone ligands benefit from the inclusion of electron-donating moieties, such as aromatic rings and electron-rich hetero atoms [77, 78].

4 Conclusion

In this section, we provide three ligands (Lph, Lme, and Lph) were synthesized and characterized. The Cu(II) complex of the three ligands (Lph, Lme, and Lph) is synthesized and characterized. The three-dimensional structure

of the synthesized molecules was verified using density functional theory methods (DFT). Adsorption of Cu(II) from aqueous solutions onto ligands was studied under a wide variety of circumstances. Adsorption behaviour was studied in relation to initial metal concentration (10–100 ppm), hydrazone ligand weight (0.1–1.0 gm), and contact time. Quick equilibrium was attained by the adsorption process after about an hour. A pH of 8.0 was determined to be ideal with a metal ion concentration of 60 ppm. In addition, spectroscopic analysis was performed to get insight into the iodine-uptake behaviour of the hydrazone ligands. At 8 h, the elimination efficiency (E , %) of hydrazone ligands peaked and subsequently steadily decreased to reach equilibrium at 25 h.

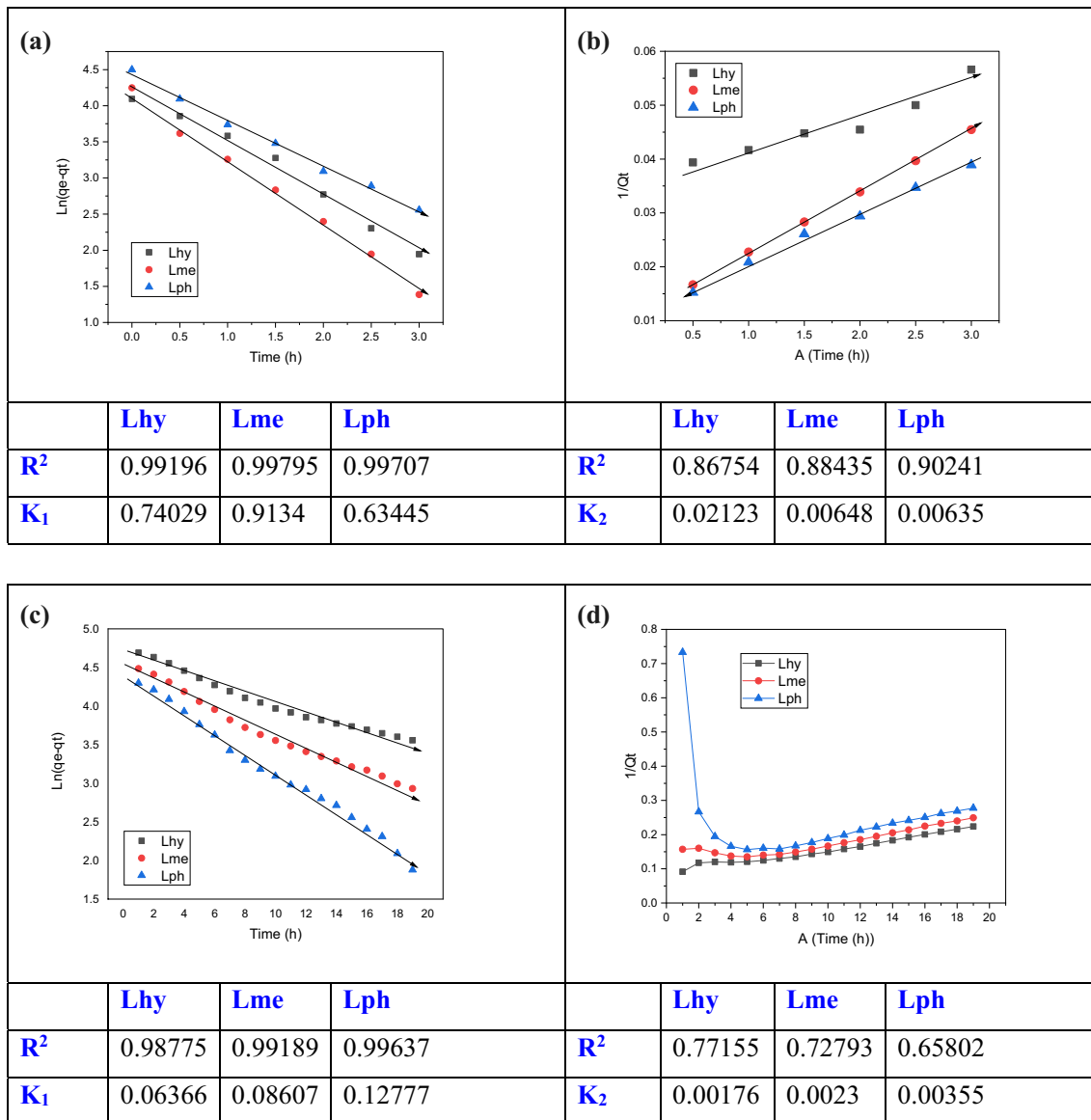


Fig. 7 pseudo-first-order model for Cu(II) (a), I₂ (b); and pseudo-second-order model for Cu(II) (c), I₂ (d)

Acknowledgements The author acknowledges Albaha University in providing the facilities for the present work.

Funding The authors declare that no funds, grants, or other support were received during the preparation of this manuscript.

Data availability All data generated or analysed during this study are included in this published article [and its supplementary information files].

Declarations

Conflict of interest There are no conflicts to declare.

Open Access This article is licensed under a Creative Commons Attribution 4.0 International License, which permits use, sharing, adaptation, distribution and reproduction in any medium or format, as long as you give appropriate credit to the original author(s) and the source, provide a link to the Creative Commons licence, and indicate if changes were made. The images or other third party material in this article are included in the article's Creative Commons licence, unless indicated otherwise in a credit line to the material. If material is not included in the article's Creative Commons licence and your intended use is not permitted by statutory regulation or exceeds the permitted use, you will need to obtain permission directly from the copyright holder. To view a copy of this licence, visit <http://creativecommons.org/licenses/by/4.0/>.

References

1. Samy F, Omar FM (2020) Synthesis, characterization, antitumor activity, molecular modeling and docking of new ligand, (2,5-pyrrole)-bis(5,6-diphenyl-[1,2,4]-triazin-3-yl)hydrazine and its complexes. *J Mol Struct* 1222:128910. <https://doi.org/10.1016/j.molstruc.2020.128910>
2. Firmino GSS, André SC, Hastenreiter Z, Campos VK, Abdel-Salam MAL, Fagundes EMS, Lessa JA (2019) In vitro assessment of the cytotoxicity of gallium(III) complexes with Isoniazid-derived hydrazones: effects on clonogenic survival of HCT-116 cells. *Inorg Chim Acta* 497:119079
3. Abd-Elzaher MM, Labib AA, Mousa HA, Moustafa SA, Abdallah MM (2014) Synthesis, characterization and cytotoxic activity of ferrocenyl hydrazone complexes containing a furan moiety. *Res Chem Intermed* 40:1923–1936
4. Samy F, Seleem HS, Taha A, Shebl M, Hanafy FI (2019) PH-metric and Theoretical Studies of The Complexation of 2-[α -(*o*-hydroxyphenyl) ethylidenehydrazino]-4, 6-dimethylquinoline and 2-[α -(*o*-methoxyphenyl) methylidenehydrazino]-4, 6-dimethylquinoline. *Egypt J Chem* 62:691–705
5. Samy F, Taha A, Seleem HS, Ramadan AAT (2020) pH-Metric studies of (2-pyrrole)-(5, 6-diphenyl-[1, 2, 4]-triazin-3-yl) hydrazone with inner transition metals. *Egypt J Chem*. <https://doi.org/10.21608/EJCHEM.2020.12631.1783>
6. Aslkhademi S, Noshiranzadeh N, Sadjadi MS, Mehrani K, Farhadyar N (2019) Synthesis, crystal structure and investigation of the catalytic and spectroscopic properties of a Zn (II) complex with coumarin-hydrazone ligand. *Polyhedron* 160:115–122
7. Taha A, Farag AAM, Adly OMI, Roushdy N, Shebl M, Ahmed HM (2017) Synthesis, spectroscopic, DFT and optoelectronic studies of 2-benzylidene-3-hydroxy-1-(5, 6-diphenyl-1, 2, 4-triazine-3-yl) hydrazine metal complexes. *J Mol Struct* 1139:31–42
8. Taha A, Farag AAM, Adly OMI, Roushdy N, Shebl M, Ahmed HM (2017) Photoresponse and DFT studies of new synthesized 2-benzylidene-3-hydroxy-1-(5, 6-diphenyl-1, 2, 4-triazine-3-yl) hydrazine and optical sensor application. *J Mol Struct* 1142:66–72
9. Shebl M, Khalil SME, Kishk MAA, El-Mekkawi DM, Saif M (2019) New less toxic zeolite-encapsulated Cu (II) complex nanomaterial for dual applications in biomedical field and wastewater remediation. *Appl Organometal Chem* 33:e5147
10. Mohanraj M, Ayyannan G, Raja G, Jayabalakrishnan C (2016) Synthesis, characterization, DNA binding, DNA cleavage, antioxidant and in vitro cytotoxicity studies of ruthenium (II) complexes containing hydrazone ligands. *J Coord Chem* 69:3545–3559
11. Jayanthi E, Anusuya M, Bhuvanesh NSP, Khalil KA, Dharmaraj N (2015) Synthesis and characterization of ruthenium (II) hydrazone complexes as anticancer chemotherapeutic agents: in vitro DNA/BSA protein binding and cytotoxicity assay. *J Coord Chem* 68:3551–3565
12. Samy F, Taha A (2018) Synthesis, spectroscopic, biological and theoretical studies of nano complexes derived from triazine hydrazone. *Egypt J Chem* 61:731–746
13. Pahonțu E, Ilieș DC, Shova S, Oprean C, Păunescu V, Olaru OT, Rădulescu FȘ, Gulea A, Roșu T, Drăgănescu D (2017) Synthesis, characterization, antimicrobial and antiproliferative activity evaluation of Cu(II), Co(II), Zn(II), Ni(II) and Pt(II) complexes with isoniazid-derived compound. *Molecules* 22:650
14. Samy F, Shebl M. 2020. *Appl. Organometal. Chem.*, 34:e5502
15. Mogharbel AT, Hossan A, Abualnaja MM, Aljuhani E, Pashameah R, Alrefae SH, Abumelha HM, El-Metwaly NM (2023) Green synthesis and characterization of new carbothioamide complexes; cyclic voltammetry and DNA/methyl green assay supported by silico ways versus DNA-polymerase. *Arab J Chem* 16(7):104807. <https://doi.org/10.1016/j.arabjc.2023.104807>
16. Alkhamis K, Alatawi NM, Alsoliemy A et al (2023) Synthesis and investigation of bivalent thiosemicarbazone complexes: conformational analysis, methyl green DNA binding and in-silico studies. *Arab J Sci Eng* 48:273–290. <https://doi.org/10.1007/s13369-022-06941-z>
17. Saber RW, Abou-Melha K, El-Metwaly N (2022) Synthesis of new Cr(III) complexes derived from antipyrine-based ligands: Elucidation, conformation, cytotoxicity and genotoxicity via in-vitro and in-silico approaches. *J Mol Liquids* 359:119361. <https://doi.org/10.1016/j.molliq.2022.119361>
18. Sharma P, Dutta D, Udayan A, Kumar S (2021) Industrial wastewater purification through metal pollution reduction employing microbes and magnetic nanocomposites. *J Environ Chem Eng* 9:106673. <https://doi.org/10.1016/j.jece.2021.106673>
19. Mahmood Q, Rashid A, Ahmad SS, Azim MR, Bilal M (2021) Current status of toxic metals addition to environment and its consequences. In: Anjum N, Ahmad I, Pereira M, Duarte A, Umar S, Khan N (eds) *The plant family brassicaceae environmental pollution*. Springer, Dordrecht. https://doi.org/10.1007/978-94-007-3913-0_2
20. Mitra S, Chakraborty AJ, Tareq AM, Emran TB, Nainu F, Khusro A, Idris AM, Khandaker MU, Osman H, Alhumaydhi FA, Simal-Gandara J (2022) Impact of heavy metals on the environment and human health: novel therapeutic insights to counter the toxicity. *J King Saud Univ - Sci* 34:101865. <https://doi.org/10.1016/j.jksus.2022.101865>
21. Qasem NAA, Mohammed RH, Lawal DU (2021) Removal of heavy metal ions from wastewater: a comprehensive and critical review. *npj Clean Water*. <https://doi.org/10.1038/s41545-021-00127-0>
22. Lupa L, Cocheci L, Dobos AM, Onofrei MD, Negrea P, Filimon A (2022) Metal ions removal from contaminated water using membranes functionalized with ionic liquids. *Water* 14:4105. <https://doi.org/10.3390/w14244105>
23. Juang RS, Shiau RC (2000) Metal removal from aqueous solutions using chitosan-enhanced membrane filtration. *J Membr Sci* 165(2):159–167
24. Saleh TA, Mustaqeem M, Khaled M (2022) Water treatment technologies in removing heavy metal ions from wastewater: a review. *Environ Nanotechnol Monitor Manag* 17:100617. <https://doi.org/10.1016/j.enmm.2021.100617>
25. Esalah JO, Weber ME, Vera JH (1999) Removal of lead from aqueous solutions by precipitation with sodium di-(*n*-octyl) phosphinate. *Sep Purif Technol* 18(1):25–36
26. Kumar P, Pournara A, Kim K-H, Bansal V, Rapti S, Manos MJ (2017) Metal-organic frameworks: Challenges and opportunities for ion-exchange/sorption applications. *Prog Mater Sci*. <https://doi.org/10.1016/j.pmatsci.2017.01.002>
27. El Samrani AG, Lartiges BS, Villiéras F (2008) Chemical coagulation of combined sewer overflow: heavy metal removal and treatment optimization. *Water Res* 42(4–5):951–960
28. Inyang MI, Gao B, Yao Y, Xue Y, Zimmerman A, Mosa A, Pullamannappallil P, Ok YS, Cao X (2016) A review of biochar as a low-cost adsorbent for aqueous heavy metal removal. *Crit Rev Environ Sci Technol* 46:406–433. <https://doi.org/10.1080/10643389.2015.1096880>
29. Benito Y, Ruiz ML (2002) Reverse osmosis applied to metal finishing wastewater. *Desalination* 142(3):229–234
30. De Los Ríos AP et al (2013) On the selective separation of metal ions from hydrochloride aqueous solution by pertraction through supported ionic liquid membranes. *J Membr Sci* 444:469–481

31. Gupta SK, Rathore NS, Sonawane JV et al (2007) Dispersion-free solvent extraction of U(VI) in macro amount from nitric acid solutions using hollow fiber contactor. *J Membr Sci* 300(1–2):131–136
32. Yurdakoç M, Seki Y, Karahan S, Yurdakoç K (2005) Kinetic and thermodynamic studies of boron removal by Siral 5, Siral 40, and Siral 80. *J Colloid Interface Sci* 286(2):440–446
33. Donia AM, Atia AA, Elwakeel KZ (2008) Selective separation of mercury(II) using magnetic chitosan resin modified with Schiff's base derived from thiourea and glutaraldehyde. *J Hazard Mater* 151(2–3):372–379
34. Wan L, Wang Y, Qian S (2002) Study on the adsorption properties of novel crown ether crosslinked chitosan for metal ions. *J Appl Polym Sci* 84(1):29–34
35. Sheikh RA, Wani MY, Shreaz S, Hashmi AA (2016) Synthesis, characterization and biological screening of some Schiff base macrocyclic ligand based transition metal complexes as antifungal agents. *Arab J Chem* 9(Supplement 1):S743–S751. <https://doi.org/10.1016/j.arabjc.2011.08.003>
36. Sanz D, Perona A, Claramunt RM, Elguero J (2005) Synthesis and spectroscopic properties of Schiff bases derived from 3-hydroxy-4-pyridinecarboxaldehyde. *Tetrahedron* 61(1):145–154
37. Olie GH, Olive S (1984) The chemistry of the catalyzes hydrogenation of carbon monoxide. Springer, Berlin, Germany
38. Taha NE (2009) Synthesis, characterization, photophysical and computational study of Schiff base ligands and their Zn (II) complexes [Ph.D. thesis], University Sains Malaysia, Kuala Lumpur, Malaysia, 2009, Thesis submitted in fulfillment of the requirements for the degree of Doctor of Philosophy.
39. Curini M, Epifano F, Maltese F, Marcotullio MC (2002) Novel chiral Schiff base ligands from amino acid amides and salicylaldehyde. *Tetrahedron Lett* 43(21):3821–3823
40. Kulkarni AD, Patil SA, Badami PS (2009) Electrochemical properties of some transition metal complexes: synthesis, characterization and in-vitro antimicrobial studies of Co (II), Ni (II), Cu (II), Mn (II) and Fe (III) complexes. *Int J Electrochem Sci* 4:717–729
41. Yoe JH, Jones AL (1944) Colorimetric determination of iron with disodium-1,2-dihydroxybenzene-3,5-disulfonate. *Ind Eng Chem (Analyst Ed)* 16:111–115
42. R. ElShiekh, M. Akl, A. Gouda and W. Ali, *J. Am. Sci.* 7(4) (2011) 797–807.
43. Shah SS and Parmar RG. 2011 *Der Pharma Chemica*, 3(1): 318–321
44. Job P. 1928. *Ann Chem*, 9:113–203
45. Issa RM, Hassanein AA, El-Mehasseb IM, El-Wadoud RIA. 2006 *Spectrochimica Acta Part A* 65: 206–214
46. Hay PJ, Wadt WR (1985) Ab initio effective core potentials for molecular calculations. Potentials for the transition metal atoms Sc to Hg. *J Chem Phys* 82:270–283
47. Elkanzi NAA, Ali AM, Albqmi M, Abdou A (2022) New benzimidazole-based Fe (III) and Cr (III) complexes: characterization, bioactivity screening, and theoretical implementations using DFT and molecular docking analysis. *Appl Organomet Chem* 36(11):e6868. <https://doi.org/10.1002/aoc.6868>
48. Frisch MJ, Trucks GW, Schlegel HB, Scuseria GE, Robb MA, Cheeseman JR et al. 2004 Gaussian 03, Revision of C.01. Wallingford CT: Gaussian Inc
49. Kh Shokr E, Kamel MS, Abdel-Ghany H, Remaily MA, Abdou A (2022) Synthesis, characterization, and DFT study of linear and non-linear optical properties of some novel thieno[2,3-b] thiophene azo dye derivatives. *Mater Chem Phys* 290:126646. <https://doi.org/10.1016/j.matchemphys.2022.126646>
50. Abu-Dief AM, Alotaibi NH, Al-Farraj ES, Qasem HA, Alzahrani S, Mahfouz MK, Abdou A (2022) Fabrication, structural elucidation, theoretical, TD-DFT, vibrational calculation and molecular docking studies of some novel adenine imine chelates for biomedical applications. *J Mol Liquids* 365:119961. <https://doi.org/10.1016/j.molliq.2022.119961>
51. Duan SX, Tang RF, Xue ZC, Zhang XX, Zhao YY, Zhang W et al (2015) Effective removal of Pb(II) using magnetic Co_{0.6}Fe_{2.4}O₄ micro-particles as the adsorbent: synthesis and study on the kinetic and thermodynamic behaviors for its adsorption. *Colloids Surf A* 469:211–223. <https://doi.org/10.1016/j.colsurfa.2015.01.029>
52. Neena S, Sunita H, Jyoti S, Vanita P, Agarwala BV (1992) Coordinative capabilities of acido anions in metal complexes of isatin and vanillin derivatives. *Synth React Inorg Met-Org Chem* 22:1283
53. Nakamoto K (1970) Infrared spectra of Inorganic and coordination compounds. Wiley-Interscience, New York
54. Murukan B, Bhageerethi SK, Kochukittan M. 2007. *J Coord Chem*, 60(15):1607
55. Cerchiaro G, Saboya PL, Ferreira AMC, Tomazela DM, Eberlin MN (2004) Keto-enolic equilibria of an isatin-schiff base copper(II) complex and its reactivity toward carbohydrate oxidation. *Tran Met Chem* 29:495
56. Hatzidimitriou A, Bolos CA (1998) The effect of chelate rings on the structure of copper(II) compounds with triamine derivatives. The crystal structure of [Cu(dptSS)Cl₂]. *Polyhedron* 17:1779
57. El Shiekh R, Akl M, Gouda A and Ali W. 2011. *J Am Sci* 7(4):797–807
58. Issa RM, Hassanein AA, El Mehasseb IM, Abed RI, Wadoud El (2006) UV-vis, IR and ¹H NMR spectroscopic studies of some 6-chloro,2-pyridyl hydrazones. *Spectrochimica Acta Part A* 65:206–214
59. Abdel-Rahman LH, El-Khatib RM, Nassr LAE, Abu-Dief AM (2013) Synthesis, physicochemical studies, embryos toxicity and DNA interaction of some new Iron(II) Schiff base amino acid complexes. *J Mol Struct* 1040:9–18
60. Jadumani Singh L and Manihar Singh AK. 2006. *J. Chem. Pharm. Res.* 3(6):1022–1027.
61. Kaur R, Sekhon BS (2006) Stability constants of 5-carboxyuracil and 5-carboxy-2-thiouracil with some metal ions. *J Indian Chem Soc* 83:645
62. Kiranmai K, Prashanthi Y, Chityala VK and Shivaraj, *J. Chem. Pharm. Res.*, 2011, 3(5), 226–233
63. Gordon M (1992) Barrow, physical chemistry, 5th edn. Tata McGraw-Hill Publishing Co., Ltd., New Delhi, p 191
64. Williams RSP 1954 *J Phys Chem.* 58, 12
65. El-Trass A, ElShamy H, El-Mehasseb I, El-Kemary M (2012) CuO nanoparticles: Synthesis, characterization, optical properties and interaction with amino acids. *App Surface Sci* 258:2997–3001
66. Li SZ, Zhang H, Ji YJ (2004) CuO nanodendrites synthesized by a novel hydrothermal route. *Nanotech* 15:1428–1435
67. Al-Fakeh MS, Alsikhan MA, Alnawmasi JS (2023) Physico-chemical study of Mn(II), Co(II), Cu(II), Cr(III), and Pd(II) complexes with schiff-base and aminopyrimidyl derivatives and anti-cancer, antioxidant antimicrobial applications. *Molecules* 28(6):2555. <https://doi.org/10.3390/molecules28062555>
68. Moustafa IML, Magda H (2017) Synthesis, spectroscopic studies and biological evaluation of Co(II), Ni(II), Cu(II) and Zr(IV) complexes of azo dyes and thiamine hydrochloride as antimicrobial agents. *Mod Chem Appl* 5:1–7
69. Elkanzi NAA, Hrichi H, Salah H, Albqmi M, Ali AM, Abdou A (2023) Synthesis, physicochemical properties, biological, molecular docking and DFT investigation of Fe(III), Co(III), Ni(II), Cu(II) and Zn(II) complexes of the 4-[(5-oxo-4,5-dihydro-1,3-thiazol-2-yl)hydrazono]methyl]phenyl 4-methylbenzenesulfonate Schiff-base ligand. *Polyhedron* 230:116219. <https://doi.org/10.1016/j.poly.2022.116219>

70. Zhou Z, Parr RG (1990) Activation hardness: new index for describing the orientation of electrophilic aromatic substitution. *J Am Chem Soc* 112:5720–5724
71. Sen KD, Mingos DMP (1993) *Structure and bonding: chemical hardness*, vol 80. Springer, Berlin
72. Parr RG, Yang W (1989) *Density functional theory of atoms and molecules*. Oxford University Press, Oxford
73. Geerlings P, de Proft F, Langenaeker W (2003) *Chem Rev* 103:1793
74. Robati D (2013) Pseudo-second-order kinetic equations for modeling adsorption systems for removal of lead ions using multi-walled carbon nanotube. *J Nanostruct Chem* 3:55. <https://doi.org/10.1186/2193-8865-3-55>
75. Mathai CJ, Saravanan S, Anantharaman MR, Venkitachalam S, Jayalekshmi S (2002) Effect of iodine doping on the bandgap of plasma polymerized aniline thin films. *J Phys D Appl Phys* 35:2206–2210
76. Yang Y et al (2019) Insight into volatile iodine uptake properties of covalent organic frameworks with different conjugated structures. *J Solid State Chem* 279:120979
77. Abdelmoaty YH, Tessema TD, Choudhury FA, El-Kadri OM, El-Kaderi HM (2018) Nitrogen-rich porous polymers for carbon dioxide and iodine sequestration for environmental remediation. *ACS Appl Mater Interfaces* 10:16049–16058
78. Sabri MA, Al-Sayah MH, Sen S, Ibrahim TH, El-Kadri OM (2020) Fluorescent aminated linked porous organic polymer for reversible iodine capture and sensing. *Sci Rep* 10:1–11

Publisher's Note Springer Nature remains neutral with regard to jurisdictional claims in published maps and institutional affiliations.